Simultaneous Finite Element Computation of Direct and Diffracted Flow Noise in Domains with Static and Moving Walls

Oriol Guasch, Arnau Pont, Joan Baiges and Ramon Codina

Abstract Curle's acoustic analogy allows one to compute aerodynamic noise due to flow motion in the presence of rigid bodies. However, the strength of the dipolar term in the analogy depends on the values of the total flow pressure on the body's surface. At low Mach numbers, that pressure cannot be obtained from the computational fluid dynamics (CFD) simulation of an incompressible flow, because the acoustic component cannot be captured. To circumvent this problem, and still being able to separate the flow and body noise contributions at a far-field point, an alternative approach was recently proposed which does not rely on an integral formulation. Rather, the acoustic pressure is split into incident and diffracted components giving rise to two differential acoustic problems that are solved together with the flow dynamics, in a single finite element computational run. In this work, we will revisit the acoustics of that approach and show how it can be extended to predict the flow noise generated in domains with moving walls.

Keywords Computational aeroacoustics · Flow noise · Finite elements Arbitrary Lagrangian–Eulerian · Diffraction · Acoustic analogy

1 Introduction

For low Mach number flows, hybrid approaches have become the most widespread formulations in computational aeroacoustics (CAA) (see e.g. [3]). The reason is that, along with the computational cost, the strong disparity between the flow speed and the speed of sound leads to convergence problems when attempting direct noise

O. Guasch (✉)
GTM-Grup de Recerca en Tecnologies Mèdia, La Salle, Universitat Ramon Llull, C/Quatre Camins 30, 08022 Barcelona, Catalonia, Spain
e-mail: oguasch@salle.url.edu
URL: http://users.salleurl.edu/~oguasch/

A. Pont · J. Baiges · R. Codina
Universitat Politècnica de Catalunya, C/Jordi Girona 1-3, Edifici C1, 08034 Barcelona, Catalonia, Spain

E. Ciappi et al. (eds.), *Flinovia—Flow Induced Noise and Vibration Issues and Aspects-II*,
https://doi.org/10.1007/978-3-319-76780-2_12

computations (DNC), which rely on the full compressible Navier–Stokes equations (see e.g. [4]). As opposed to this, hybrid approaches consist of a first computational fluid dynamics (CFD) simulation of the incompressible Navier–Stokes equations. This serves to determine the source terms of an acoustic analogy, Lighthill's being the most celebrated one [29]. The analogy is then solved using an integral formulation, making use of Green functions. If rigid bodies are present within the flow, one usually resorts to Curle's analogy [12] and, if those can move, to its generalization, namely the Ffowcs Williams–Hawkings equation [36].

From a computational point of view, hybrid approaches imply working with two codes; typically a finite element method (FEM) one for the CFD and a boundary element method (BEM) for the acoustics. If one is not interested in the solution at large distances from the aeroacoustic sources, the two codes can be avoided and one can simply use FEM to get the flow and the acoustic fields (see e.g. [19, 20, 28, 31]). This has the advantage of only needing one computational code, but the disadvantage is that one can no longer separate the noise contributions, at a far-field point, from the unsteady flow (quadrupolar term in Curle's analogy), and from the rigid body itself (dipolar term in Curle's analogy). However, Curle's analogy is not free of problems in low Mach number simulations. This is because only incompressible pressure fluctuations can be recovered from incompressible CFD computations, not the acoustic ones. Unfortunately, the latter are also needed on the rigid surface for a proper implementation of Curle's analogy.

To circumvent this difficulty, make use of a single FEM code for both the flow and the acoustic fields, and be able to distinguish between the direct flow and the body noise contributions, a different approach was proposed in [21]. In that work, advantage was taken from the fact that the dipolar term in Curle's analogy corresponds to the turbulent noise diffracted by the rigid body (see e.g. [17]). The acoustic pressure in Lighthill's acoustic analogy was split into a direct plus diffracted components as in classical diffraction problems. At every time step of a single FEM run, the incompressible Navier–Stokes equations were first solved. The resulting velocity field was then inserted as a source term in a wave equation for the direct incident acoustic pressure, and that was finally used in the boundary conditions of another wave equation for the diffracted acoustic pressure. Some benchmark cases to test the methodology were presented in [21], and in [33] the approach has been recently applied to voice production, for better understanding the generation mechanisms of sibilant [s].

In this work, we will revisit the main results in [21] and show how they can be extended to account for the prediction of flow noise in domains with moving walls. Focus will be placed on the acoustics formulation rather than on the CFD. Working with moving domains will require setting the governing equations in an arbitrary Lagrangian–Eulerian (ALE) frame of reference. As we shall see, the irreducible wave equation will be no longer valid in this case, and we will have to work with the wave equation in mixed form (see e.g. [7]). The splitting into incident and diffracted components in [21] will be applied to the ALE mixed wave equation and we will show how to solve it resorting to the stabilized FEM in [18]. Some numerical examples will be presented. First, we will briefly summarize the case with static boundaries

in [33], which consists of a large-scale three-dimensional CAA simulation for the production of the sibilant [s]. Second, we will present a case with moving walls which comprises a flow exiting a two-dimensional duct, with a teeth-shaped obstacle at its end that evolves from an almost closed aperture to an open one.

2 Diffracted Sound and Curle's Analogy

To begin with, let us consider the problem depicted in Fig. 1. A low Mach flow is impinging on a rigid body Ω_b, which we assume stationary for the moment, and a wake develops past the body. As a result, aerodynamic noise is generated due to unsteady flow motion. At a far-field point in Ω_{ac}, the acoustic pressure, $p(\boldsymbol{x}, t)$, will have a contribution directly stemming from the flow motion and a contribution arising from the diffraction of the flow noise by the body. Assuming that one has already performed a CFD computation to get the flow velocity and pressure, Curle's analogy can be used to determine those acoustic contributions with the sole use of the free-space Green function for the wave equation. Curle's final integral formulation [12] for the acoustic pressure reads (neglecting the viscous stress tensor contributions),

$$p\,(\boldsymbol{x}, t) = \rho_0 \partial_{ij}^2 \int_{\Omega_{ac}} \frac{1}{4\pi\,|\boldsymbol{x} - \boldsymbol{y}|} \left[u_i^0 u_j^0\right]_{t'} d^3\boldsymbol{y} - \partial_i \int_{\Gamma_b} \frac{1}{4\pi\,|\boldsymbol{x} - \boldsymbol{y}|} [P]_{t'} n_i d^2\boldsymbol{y}. \quad (1)$$

Following the convention for retarded potentials, the squared brackets in the equation stand for evaluation at the retarded time $t' := t - |\boldsymbol{x} - \boldsymbol{y}|/c_0$. The parameters

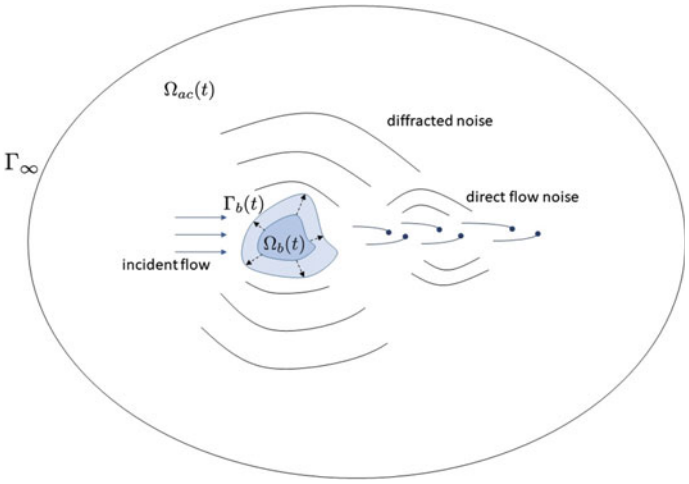

Fig. 1 Computational domain. The body $\Omega_b(t)$ can change its shape with time and consequently so does $\Omega_{ac}(t)$

c_0 and ρ_0 respectively denote the speed of sound and the mean air density, whereas ∂_i designates the first-order spatial derivative with respect to the component x_i, and ∂^2_{ij} represents the second-order cross-derivative with respect to x_i and x_j.

The first integral in (1) provides the direct flow noise contribution to $p(\boldsymbol{x}, t)$ assuming the low Mach number approximation to Lighthill's tensor, namely $\mathcal{S}^0 = \rho_0 \partial^2_{ij}(u^0_i u^0_j)$, with $\boldsymbol{u}^0(\boldsymbol{x}, t)$ denoting the incompressible flow velocity. The second integral contains the contribution from the sound diffracted by the rigid body [10, 13, 17, 21]. While $\boldsymbol{u}^0(\boldsymbol{x}, t)$ in the first integral can be obtained from an incompressible CFD simulation, the problem is that this is not possible for the pressure $P(\boldsymbol{x}, t)$ in the second integral, because $P(\boldsymbol{x}, t)$ accounts for the total compressible pressure at the body's boundary.

3 Splitting the Acoustic Pressure into Incident and Diffracted Components

3.1 General Linear Acoustic Wave Operator

To avoid the difficulties with Curle's analogy described in the preceding section and still being able possible to separate the direct and diffracted flow noise contributions using a single FEM code, an alternative was proposed in [21]. To introduce it, let us consider a more general situation for the aeroacoustic problem presented in Fig. 1, also in the framework of acoustic analogies.

Assume again that we have already computed an aeroacoustic source term $\mathcal{S}$ from a CFD simulation of the incompressible Navier–Stokes equations (for the time being not necessarily the low Mach approximation to Lighthill's tensor). We will first state the problem of computing the aerodynamic noise generated by such a term in an acoustic computational domain Ω_{ac}. Suppose that the acoustic wave propagation is driven by a linear wave operator $\mathcal{L}$ acting on the acoustic pressure p (explicit indication of dependence on space and time will be hereafter omitted), that B_b represents another linear operator defining the boundary conditions on the body immersed in the flow, and that B_∞ stands for a third linear operator accounting for a non-reflecting boundary condition at Γ_∞ (see Fig. 1). The acoustic pressure p in Ω_{ac} can be obtained from the solution of

$$\mathcal{L}p = \mathcal{S} \quad \text{in } \Omega_{ac},\ t > 0, \tag{2a}$$

$$\nabla p \cdot \boldsymbol{n} = B_b p \quad \text{on } \Gamma_b,\ t > 0, \tag{2b}$$

$$\nabla p \cdot \boldsymbol{n} = B_\infty p \quad \text{on } \Gamma_\infty,\ t > 0, \tag{2c}$$

$$p(\boldsymbol{x}, 0) = 0,\ \partial_t p(\boldsymbol{x}, 0) = 0 \quad \text{in } \Omega_{ac},\ t = 0. \tag{2d}$$

To determine, at a given position, the separate acoustic pressure contribution of the direct sound generated by the aeroacoustic source $\mathcal{S}$, say p_i, from that diffracted

by the rigid body, p_d, we can split the total acoustic pressure as $p = p_i + p_d$ and substitute into (2). This results in the following problem for p_i,

$$\mathcal{L}p_i = \mathcal{S} \quad \text{in } \Omega_{ac} \cup \Omega_b,\ t > 0, \tag{3a}$$

$$\nabla p_i \cdot \boldsymbol{n} = B_\infty p_i \quad \text{on } \Gamma_\infty,\ t > 0, \tag{3b}$$

$$p_i(\boldsymbol{x}, 0) = 0,\ \partial_t p_i(\boldsymbol{x}, 0) = 0 \quad \text{in } \Omega_{ac} \cup \Omega_b\ t = 0, \tag{3c}$$

which once solved can be used to obtain p_d,

$$\mathcal{L}p_d = 0 \quad \text{in } \Omega_{ac},\ t > 0, \tag{4a}$$

$$\nabla p_d \cdot \boldsymbol{n} - B_b p_d = -\nabla p_i \cdot \boldsymbol{n} + B_b p_i \quad \text{on } \Gamma_b,\ t > 0, \tag{4b}$$

$$\nabla p_d \cdot \boldsymbol{n} = B_\infty p_d \quad \text{on } \Gamma_\infty,\ t > 0, \tag{4c}$$

$$p_d(\boldsymbol{x}, 0) = 0,\ \partial_t p_d(\boldsymbol{x}, 0) = 0 \quad \text{in } \Omega_{ac},\ t = 0. \tag{4d}$$

Note that we can recover the original problem (2) from the summation of problems (3) and (4). To solve (3), we need to remove Ω_b from the computational domain and make the computations as if the body was absent. Once we get p_i, we include the body back in the computational domain and use p_i at its boundary Γ_b, to compute the diffracted pressure p_d.

The above splitting procedure is nothing but the standard way to deal with diffraction and scattering problems in acoustics (see e.g. [30]). As explained in the Introduction, the novelty in [21] consisted in exploiting that factorization in CAA to avoid the problems encountered when applying Curle's analogy to low-speed subsonic flows.

3.2 Domains with Static Walls

A first application of the splitting approach (3)–(4) is that of finding the incident and diffracted flow noise contributions at a far-field point. Let us take the irreducible wave equation as the linear operator in (2), i.e. $\mathcal{L} \equiv c_0^{-2}\partial_{tt}^2 - \nabla^2$, and suppose the body to be acoustically rigid. Assume once more that we have obtained an incompressible pressure field, p^0, and an incompressible velocity field, $\boldsymbol{u}^0$, from the solution of the incompressible Navier–Stokes equations. We could then build an aeroacoustic source term by taking, for instance, $\mathcal{S}^0 = \rho_0 \partial_{ij}^2 (u_i^0 u_j^0)$, which as said before is nothing but the approximation to Lighthill's tensor at low Mach numbers. In the case of sound propagating in non-quiescent flow areas, however, convective and refraction effects should be removed from the source term and incorporated into the wave operator. Otherwise, non-acoustic pressure fluctuations that do not correspond to proper sound could manifest in the solution (this is usually referred to as *pseudosound*, see e.g. [11]). Several options exist to remedy the situation that range from the linearized Euler equations (LEE) [2], to the acoustic perturbation equations (APE) which filter the LEE to get rid of its entropy and vorticity modes [15]. A simplified version

of the APE for low Mach numbers can be found in [22, 23]. In the case of almost negligible convection velocities, the latter reduces to Roger's acoustic analogy in [34] with source term $\mathcal{S}^0 = c_0^{-2}\partial_{tt}^2 p^0$. The latter allows one to filter some pseudosound and will be considered in this work together with Lighthill's one.

With the above considerations, the splitting into incident and diffracted components yields the following particular cases of problems (3) and (4),

$$\frac{1}{c_0^2}\partial_{tt}^2 p_i - \nabla^2 p_i = \mathcal{S}^0 \quad \text{in } \Omega_{ac} \cup \Omega_b,\ t > 0, \tag{5a}$$

$$\nabla p_i \cdot \boldsymbol{n} = \frac{1}{c_0}\partial_t p_i \quad \text{on } \Gamma_\infty,\ t > 0, \tag{5b}$$

$$p_i(\boldsymbol{x}, 0) = 0,\ \partial_t p_i(\boldsymbol{x}, 0) = 0 \quad \text{in } \Omega_{ac} \cup \Omega_b\ t = 0, \tag{5c}$$

and

$$\frac{1}{c_0^2}\partial_{tt}^2 p_d - \nabla^2 p_d = 0 \quad \text{in } \Omega_{ac},\ t > 0, \tag{6a}$$

$$\nabla p_d \cdot \boldsymbol{n} = -\nabla p_i \cdot \boldsymbol{n} \quad \text{on } \Gamma_b,\ t > 0, \tag{6b}$$

$$\nabla p_d \cdot \boldsymbol{n} = \frac{1}{c_0}\partial_t p_d \quad \text{on } \Gamma_\infty,\ t > 0, \tag{6c}$$

$$p_d(\boldsymbol{x}, 0) = 0,\ \partial_t p_d(\boldsymbol{x}, 0) = 0 \quad \text{in } \Omega_{ac},\ t = 0. \tag{6d}$$

Note that (5b) and (6c) correspond to the Sommerfeld radiation condition that prevents outward propagating waves to be reflected back from the outer boundaries of the computational domain.

The above formulation was used in [21] to compute the turbulent and diffracted components of sound generated past a two-dimensional cylinder (aeolian tones), and also to determine the incident and diffracted flow noise contributions of an obstacle placed at the exit of a three-dimensional duct. More recently, the methodology in [21] has been applied to voice production in [33] to determine the contributions of the sound diffracted by the upper teeth in the generation of sibilant /s/ (see Sect. 5.1).

3.3 Domains with Moving Walls

The main goal of the present work is to show how to extend the above splitting procedure to the case of flow noise generated in domains with moving walls. As mentioned, an example could be that of the aeroacoustics of a flow emanating from a duct with a time-varying exit section. Typical cases also arise once more in voice production, for example, when pronouncing a syllable that involves a sibilant sound.

When dealing with acoustic waves propagating in moving domains, it becomes no longer possible to resort to the acoustic wave equation in irreducible form. The

linearized continuum and momentum conservation equations used to derive the latter need to be expressed in an ALE frame of reference, which precludes obtaining a scalar wave equation for the acoustic pressure [18]. One is then forced to work with the linearized momentum and continuity equations, sometimes referred to as the wave equation in mixed form (see e.g. [7]). This reads,

$$\frac{1}{\rho_0 c_0^2}\partial_t p + \nabla \cdot \boldsymbol{u} = Q, \tag{7a}$$

$$\rho_0 \partial_t \boldsymbol{u} + \nabla p = \boldsymbol{f}, \tag{7b}$$

where p stands anew for the acoustic pressure while $\boldsymbol{u}$ represents the acoustic particle velocity. Q denotes a volume source distribution and $\boldsymbol{f}$ an external body force per unit volume.

To express (7) in an ALE domain, a quasi-Eulerian approximation is often used [24, 27], which basically consists in expressing the time derivative of any fluid property, say g, in a referential frame moving with the domain, i.e. replacing $\partial_t g \leftarrow \partial_t g - \boldsymbol{u}_{\text{dom}} \cdot \nabla g$, while keeping the spatial derivatives Eulerian. $\boldsymbol{u}_{\text{dom}}$ denotes the domain velocity and it will be hereafter termed the mesh velocity, because it corresponds to the mesh node velocities in the computational implementation. The ALE counterpart of (7) becomes

$$\frac{1}{\rho_0 c_0^2}\partial_t p - \frac{1}{\rho_0 c_0^2}\boldsymbol{u}_{\text{dom}} \cdot \nabla p + \nabla \cdot \boldsymbol{u} = Q, \tag{8a}$$

$$\rho_0 \partial_t \boldsymbol{u} - \rho_0 \boldsymbol{u}_{\text{dom}} \cdot \nabla \boldsymbol{u} + \nabla p = \boldsymbol{f}. \tag{8b}$$

The source terms corresponding to Lighthill's analogy and the Roger one in [34] are given by,

$$\text{Roger's analogy:} \quad \boldsymbol{f} = \boldsymbol{0},\ Q = -(1/\rho_0 c_0^2)\left[\partial_t p^0 - \boldsymbol{u}_{\text{dom}} \cdot \nabla p^0\right], \tag{9a}$$

$$\text{Lighthill's analogy:} \quad f_i = -\rho_0 \partial_j (u_i^0 u_j^0),\ Q = 0. \tag{9b}$$

To solve (8) in a computational domain $\Omega_{ac}(t),\ t > 0$, we need to supplement the equation with appropriate boundary conditions and initial conditions. Assuming again a rigid body for simplicity, we get

$$\boldsymbol{u} \cdot \boldsymbol{n} = 0 \quad \text{on } \Gamma_b(t)\ t > 0, \tag{10a}$$

$$\boldsymbol{u} \cdot \boldsymbol{n} = \frac{1}{Z_0} p \quad \text{on } \Gamma_\infty\ t > 0, \tag{10b}$$

$$p\,(\boldsymbol{x}, 0) = 0\ \boldsymbol{u}\,(\boldsymbol{x}, 0) = \boldsymbol{0}, \quad \text{in } \Omega_{ac}(t),\ t = 0 \tag{10c}$$

where (10b) is the Sommerfeld radiation condition for the wave equation in mixed form (see e.g. [14]) and $Z_0 = \rho_0 c_0$.

We can next apply the splitting strategy into incident and diffracted fields for the ALE mixed wave Eq. (8). Notice that the general linear operator $\mathcal{L}$ in (2) herein acts both on the acoustic pressure p and on the acoustic particle velocity $\boldsymbol{u}$. Taking $\boldsymbol{u} = \boldsymbol{u}_{in} + \boldsymbol{u}_d$ and $p = p_{in} + p_d$ in (8), we get the incident field problem

$$\frac{1}{\rho_0 c_0^2}\partial_t p_{in} - \frac{1}{\rho_0 c_0^2}\boldsymbol{u}_{\text{dom}} \cdot \nabla p_{in} + \nabla \cdot \boldsymbol{u}_{in} = Q \quad \text{in } \Omega_{ac}(t) \cup \Omega_b(t),\ t > 0, \tag{11a}$$

$$\rho_0 \partial_t \boldsymbol{u}_{in} - \rho_0 \boldsymbol{u}_{\text{dom}} \cdot \nabla \boldsymbol{u}_{in} + \nabla p_{in} = \boldsymbol{f} \quad \text{in } \Omega_{ac}(t) \cup \Omega_b(t),\ t > 0, \tag{11b}$$

$$\boldsymbol{u}_{in} \cdot \boldsymbol{n} = \frac{1}{Z_0} p_{in} \quad \text{on } \Gamma_\infty,\ t > 0, \tag{11c}$$

$$p_{in}(\boldsymbol{x}, 0) = 0,\ \boldsymbol{u}_{in}(\boldsymbol{x}, 0) = \boldsymbol{0}, \quad \text{in } \Omega_{ac}(t) \cup \Omega_b(t),\ t = 0, \tag{11d}$$

and the diffracted field one,

$$\frac{1}{\rho_0 c_0^2}\partial_t p_d - \frac{1}{\rho_0 c_0^2}\boldsymbol{u}_{\text{dom}} \cdot \nabla p_d + \nabla \cdot \boldsymbol{u}_d = 0 \quad \text{in } \Omega_{ac}(t),\ t > 0, \tag{12a}$$

$$\rho_0 \partial_t \boldsymbol{u}_d - \rho_0 \boldsymbol{u}_{\text{dom}} \cdot \nabla \boldsymbol{u}_d + \nabla p_d = \boldsymbol{0} \quad \text{in } \Omega_{ac}(t),\ t > 0, \tag{12b}$$

$$\boldsymbol{u}_d \cdot \boldsymbol{n} = -\boldsymbol{u}_{in} \cdot \boldsymbol{n} \quad \text{on } \Gamma_b(t),\ t > 0, \tag{12c}$$

$$\boldsymbol{u}_d \cdot \boldsymbol{n} = \frac{1}{Z_0} p_d \quad \text{on } \Gamma_\infty,\ t > 0, \tag{12d}$$

$$p_d(\boldsymbol{x}, 0) = 0,\ \boldsymbol{u}_d(\boldsymbol{x}, 0) = \boldsymbol{0}, \quad \text{in } \Omega_{ac}(t),\ t = 0. \tag{12e}$$

The source terms Q and $\boldsymbol{f}$ in (11) need to be obtained from the solution of the incompressible Navier–Stokes in an ALE framework. Our objective is to solve the latter together with (11) and (12) in a single finite element computational run, following the strategy in [21].

4 Numerical Discretization for Waves in Moving Domains

4.1 Continuous Weak Form

The FEM discretization of Eqs. (11) and (12) relies on their weak formulation rather than on the differential one. The continuous weak forms of the equations can be found multiplying Eqs. (11a) and (12a) with a scalar test function q, and Eqs. (11b) and (12b) with a vector test function $\boldsymbol{v}$, and then integrating over the respective computational domains $\Omega_{ac}(t) \cup \Omega_b(t)$ and $\Omega_{ac}(t)$. Let us denote by $(f, g) := \int_\Omega f g d\Omega$ the integral of the product between two arbitrary functions f and g, and assume that we want to solve the problem in a given time interval $[0, T]$. The variational problems for the incident and diffracted acoustic pressure and velocity can be posed as follows.

First, find $p_{in} \in \mathcal{W}_p^{in}([0,T], V_p^{in})$ and $\boldsymbol{u}_{in} \in \boldsymbol{\mathcal{W}}_{\boldsymbol{u}}^{in}([0,T], \boldsymbol{V}_{\boldsymbol{u}}^{in})$ such that

$$\frac{1}{\rho_0 c_0^2}(\partial_t p_{in}, q) - \frac{1}{\rho_0 c_0^2}(\boldsymbol{u}_{\text{dom}} \cdot \nabla p_{in}, q) + (\nabla \cdot \boldsymbol{u}_{in}, q) = (Q, q)\ \forall\, q \in V_p^{in}, \tag{13a}$$

$$\rho_0(\partial_t \boldsymbol{u}_{in}, \boldsymbol{v}) - \rho_0(\boldsymbol{u}_{\text{dom}} \cdot \nabla \boldsymbol{u}_{in}, \boldsymbol{v}) + (\nabla p_{in}, \boldsymbol{v}) = (\boldsymbol{f}, \boldsymbol{v})\ \forall\, \boldsymbol{v} \in \boldsymbol{V}_{\boldsymbol{u}}^{in}, \tag{13b}$$

where $\mathcal{W}_p^{in}$, $\boldsymbol{\mathcal{W}}_{\boldsymbol{u}}^{in}$, V_p^{in} and $\boldsymbol{V}_{\boldsymbol{u}}^{in}$ denote appropriate functional spaces in $\Omega_{ac}(t) \cup \Omega_b(t)$, not to be detailed herein (see e.g. [18] for more details). As for the diffracted fields, we will have to find $p_d \in \mathcal{W}_p^d([0,T], V_p^d)$ and $\boldsymbol{u}_d \in \boldsymbol{\mathcal{W}}_{\boldsymbol{u}}^d([0,T], \boldsymbol{V}_{\boldsymbol{u}}^d)$ such that

$$\frac{1}{\rho_0 c_0^2}(\partial_t p_d, q) - \frac{1}{\rho_0 c_0^2}(\boldsymbol{u}_{\text{dom}} \cdot \nabla p_d, q) + (\nabla \cdot \boldsymbol{u}_d, q) = (Q, q) \quad \forall\, q \in V_p^d, \tag{14a}$$

$$\rho_0(\partial_t \boldsymbol{u}_d, \boldsymbol{v}) - \rho_0(\boldsymbol{u}_{\text{dom}} \cdot \nabla \boldsymbol{u}_d, \boldsymbol{v}) + (\nabla p_d, \boldsymbol{v}) = (\boldsymbol{f}, \boldsymbol{v}) \quad \forall\, \boldsymbol{v} \in \boldsymbol{V}_{\boldsymbol{u}}^d, \tag{14b}$$

with $\mathcal{W}_p^d$, $\boldsymbol{\mathcal{W}}_{\boldsymbol{u}}^d$, V_p^d and $\boldsymbol{V}_{\boldsymbol{u}}^d$ standing now for appropriate functional spaces in $\Omega_{ac}(t)$.

The Dirichlet boundary conditions (11c), (12c) and (12d) are to be imposed strongly on $\Gamma_b(t)$ and Γ_∞. Alternatively, one could integrate the terms $(\nabla \cdot \boldsymbol{u}_{in}, q)$ in (13a) and $(\nabla \cdot \boldsymbol{u}_d, q)$ in (14a) to impose the conditions weakly. The consequences of such an option are detailed in [1].

4.2 Finite Element Spatial Discretization

The Galerkin FEM solution to variational mixed problems like (13) and (14) is known to exhibit strong oscillations if equal order interpolations are used for the pressure and velocities (see e.g. [7, 8, 18]). One could prevent them by resorting to stabilized FEM strategies like the variational multiscale (VMS) method in [25, 26]. In this work, orthogonal subgrid scales (OSS), see [6, 9], will be used to stabilize the Galerkin FEM approach to (13) and (14), following the strategy depicted in [18].

Let us consider the finite element spaces $V_{p_h} \subset V_p$ and $\boldsymbol{V}_{\boldsymbol{u}_h} \subset \boldsymbol{V}_{\boldsymbol{u}}$ constructed from a finite element partition $\Omega^e(t)$ of $\Omega(t)$, where the index e ranges from 1 to the number of elements n_{el}. The discrete stabilized FEM approach to the incident problem (13) consists in finding $p_{in_h} \in \mathcal{W}_{p_h}^{in}([0,T], V_{p_h}^{in})$ and $\boldsymbol{u}_{in_h} \in \boldsymbol{\mathcal{W}}_{\boldsymbol{u}_h}^{in}([0,T], \boldsymbol{V}_{\boldsymbol{u}_h}^{in})$ such that

$$\frac{1}{\rho_0 c_0^2}(\partial_t p_{in_h}, q_h) - \frac{1}{\rho_0 c_0^2}(\boldsymbol{u}_{\text{dom}} \cdot \nabla p_{in_h}, q_h) + (\nabla \cdot \boldsymbol{u}_{in_h}, q_h)$$
$$+ \sum_{e=1}^{n_{el}} (\tau_p \mathcal{P}\big[- \frac{1}{\rho_0 c_0^2} \boldsymbol{u}_{\text{dom}} \cdot \nabla p_{in_h} + \nabla \cdot \boldsymbol{u}_{in_h} - Q\big], - \frac{1}{\rho_0 c_0^2} \boldsymbol{u}_{\text{dom}} \cdot \nabla q_{in_h}$$
$$+ \nabla \cdot \boldsymbol{v}_h)_{\Omega_e(t)} = (Q, q_h), \tag{15a}$$
$$\rho_0(\partial_t \boldsymbol{u}_{in_h}, \boldsymbol{v}_h) - \rho_0(\boldsymbol{u}_{\text{dom}} \cdot \nabla \boldsymbol{u}_{in_h}, \boldsymbol{v}_h) + (\nabla p_{in_h}, \boldsymbol{v}_h)$$
$$+ \sum_{e=1}^{n_{el}} (\tau_{\boldsymbol{u}} \mathcal{P}\big[- \rho_0 \boldsymbol{u}_{\text{dom}} \cdot \nabla \boldsymbol{u}_{in_h} + \nabla p_{in_h} - \boldsymbol{f}\big], - \rho_0 \boldsymbol{u}_{\text{dom}} \cdot \nabla \boldsymbol{v}_h + \nabla q_h)_{\Omega_e(t)}$$
$$= (\boldsymbol{f}, \boldsymbol{v}_h), \tag{15b}$$

for all $q_h \in V^{in}_{p_h}$ and $\boldsymbol{v}_h \in \boldsymbol{V}^{in}_{\boldsymbol{u}_h}$.

The first and fourth rows in the above equations contain the Galerkin FEM terms, whereas the second and fifth rows account for the stabilization terms. $\mathcal{P}$ in (15) stands for a projection to be applied either to scalars or vectors depending on the argument. In the OSS method, $\mathcal{P}$ is computed as $\mathcal{P} = \boldsymbol{I} - \Pi_h$, with $\boldsymbol{I}$ being the identity and Π_h the L^2-projection onto the corresponding finite element space. On the other hand, the following expressions can be obtained for the stabilization parameters τ_p and $\tau_{\boldsymbol{u}}$, (see [18])

$$\tau_p = \frac{\rho_0 c_0^2 h}{C_1 |\boldsymbol{u}_d| + c_0 C_2},$$
$$\tau_{\boldsymbol{u}} = \frac{h}{C_1 \rho_0 |\boldsymbol{u}_d| + \rho_0 c_0 C_2}, \tag{16}$$

with C_1 and C_2 being constants to be determined from numerical experiments (a value of $C_1 = C_2 = 100$ was taken in [18]).

Analogously, the discrete stabilized FEM approach to the diffraction problem (14) is that of finding $p_{d_h} \in \mathcal{W}^d_{p_h}([0, T], V^d_{p_h})$ and $\boldsymbol{u}_{d_h} \in \boldsymbol{\mathcal{W}}^d_{\boldsymbol{u}_h}([0, T], \boldsymbol{V}^d_{\boldsymbol{u}_h})$ such that

$$\frac{1}{\rho_0 c_0^2}(\partial_t p_{d_h}, q_h) - \frac{1}{\rho_0 c_0^2}(\boldsymbol{u}_{\text{dom}} \cdot \nabla p_{d_h}, q_h) + (\nabla \cdot \boldsymbol{u}_{d_h}, q_h)$$
$$+ \sum_{e=1}^{n_{el}} (\tau_p \mathcal{P}\big[- \frac{1}{\rho_0 c_0^2} \boldsymbol{u}_{\text{dom}} \cdot \nabla p_{d_h} + \nabla \cdot \boldsymbol{u}_{d_h} - Q\big], - \frac{1}{\rho_0 c_0^2} \boldsymbol{u}_{\text{dom}} \cdot \nabla q_h$$
$$+ \nabla \cdot \boldsymbol{v}_h)_{\Omega_e(t^n)} = (Q^{n+1}, q_h), \tag{17a}$$
$$\rho_0(\partial_t \boldsymbol{u}_{d_h}, \boldsymbol{v}_h) - \rho_0(\boldsymbol{u}_{\text{dom}} \cdot \nabla \boldsymbol{u}_{d_h}, \boldsymbol{v}_h) + (\nabla p_{d_h}, \boldsymbol{v}_h)$$
$$+ \sum_{e=1}^{n_{el}} (\tau_{\boldsymbol{u}} \mathcal{P}\big[- \rho_0 \boldsymbol{u}_{\text{dom}} \cdot \nabla \boldsymbol{u}_{d_h} + \nabla p_{d_h} - \boldsymbol{f}\big], - \rho_0 \boldsymbol{u}_{\text{dom}} \cdot \nabla \boldsymbol{v}_h + \nabla q_h)_{\Omega_e(t)}$$
$$= (\boldsymbol{f}, \boldsymbol{v}_h), \tag{17b}$$

for all $q_h \in V^d_{p_h}$ and $\boldsymbol{v}_h \in \boldsymbol{V}^d_{\boldsymbol{u}_h}$.

4.3 Fully Discrete Numerical Scheme

To get the final numerical scheme, we need to discretize Eqs. (15) and (17) in time. To that purpose, we split the time interval $[0\ T]$ into N equal steps $0 < t^1 < t^2 < \cdots < t^n < \cdots < t^N \equiv T$ with $\Delta t := t^{n+1} - t^n$ the time step size. For a time-dependent function $g(t)$, g^n will denote its evaluation at $t^n = n\Delta t$. A second-order backward differentiation formula (BDF2) will be used to approximate the first-order time derivative of g, which results in $\delta_t g^{n+1} := (1/2\Delta t)(3g^{n+1} - 4g^n + g^{n-1})$.

The time discrete version of the incident problem (15) then becomes

$$\begin{aligned}
&\frac{1}{\rho_0 c_0^2}(\delta_t p_{in_h}^{n+1}, q_h) - \frac{1}{\rho_0 c_0^2}(\boldsymbol{u}_{\text{dom}} \cdot \nabla p_{in_h}^{n+1}, q_h) + (\nabla \cdot \boldsymbol{u}_{in_h}^{n+1}, q_h) \\
&+ \sum_{e=1}^{n_{el}} (\tau_p \mathcal{P}\big[- \frac{1}{\rho_0 c_0^2}\boldsymbol{u}_{\text{dom}} \cdot \nabla p_{in_h}^{n+1} + \nabla \cdot \boldsymbol{u}_{in_h}^{n+1} - Q^{n+1}\big], -\frac{1}{\rho_0 c_0^2}\boldsymbol{u}_{\text{dom}} \cdot \nabla q_h \\
&+ \nabla \cdot \boldsymbol{v}_h)_{\Omega_e(t^{n+1})} = (Q^{n+1}, q_h), \qquad (18a) \\
&\rho_0(\delta_t \boldsymbol{u}_{in_h}^{n+1}, \boldsymbol{v}_h) - \rho_0(\boldsymbol{u}_{\text{dom}} \cdot \nabla \boldsymbol{u}_{in_h}^{n+1}, \boldsymbol{v}_h) + (\nabla p_{in_h}^{n+1}, \boldsymbol{v}_h) \\
&+ \sum_{e=1}^{n_{el}} (\tau_{\boldsymbol{u}} \mathcal{P}\big[- \rho_0 \boldsymbol{u}_{\text{dom}} \cdot \nabla \boldsymbol{u}_{in_h}^{n+1} + \nabla p_{in_h}^{n+1} - \boldsymbol{f}^{n+1}\big], -\rho_0 \boldsymbol{u}_d \cdot \nabla \boldsymbol{v}_h + \nabla q_h)_{\Omega_e(t^{n+1})} \\
&= (\boldsymbol{f}^{n+1}, \boldsymbol{v}_h). \qquad (18b)
\end{aligned}$$

Note that $\mathcal{P}(\delta_t p_h) = 0$ and $\mathcal{P}(\delta_t \boldsymbol{u}_h) = 0$ in (18) because we are considering orthogonal subscales.

Similarly, the time discrete version of the diffraction problem (17) is given by

$$\begin{aligned}
&\frac{1}{\rho_0 c_0^2}(\delta_t p_{d_h}^{n+1}, q_h) - \frac{1}{\rho_0 c_0^2}(\boldsymbol{u}_{\text{dom}} \cdot \nabla p_{d_h}^{n+1}, q_h) + (\nabla \cdot \boldsymbol{u}_{d_h}^{n+1}, q_h) \\
&+ \sum_{e=1}^{n_{el}} (\tau_p \mathcal{P}\big[- \frac{1}{\rho_0 c_0^2}\boldsymbol{u}_{\text{dom}} \cdot \nabla p_{d_h}^{n+1} + \nabla \cdot \boldsymbol{u}_{d_h}^{n+1} - Q^{n+1}\big], -\frac{1}{\rho_0 c_0^2}\boldsymbol{u}_{\text{dom}} \cdot \nabla q_h \\
&+ \nabla \cdot \boldsymbol{v}_h)_{\Omega_e(t^{n+1})} = (Q^{n+1}, q_h), \qquad (19a) \\
&\rho_0(\delta_t \boldsymbol{u}_{d_h}^{n+1}, \boldsymbol{v}_h) - \rho_0(\boldsymbol{u}_{\text{dom}} \cdot \nabla \boldsymbol{u}_{d_h}^{n+1}, \boldsymbol{v}_h) + (\nabla p_{d_h}^{n+1}, \boldsymbol{v}_h) \\
&+ \sum_{e=1}^{n_{el}} (\tau_{\boldsymbol{u}} \mathcal{P}\big[- \rho_0 \boldsymbol{u}_{\text{dom}} \cdot \nabla \boldsymbol{u}_{d_h}^{n+1} + \nabla p_{d_h}^{n+1} - \boldsymbol{f}^{n+1}\big], -\rho_0 \boldsymbol{u}_d \cdot \nabla \boldsymbol{v}_h + \nabla q_h)_{\Omega_e(t^{n+1})} \\
&= (\boldsymbol{f}^{n+1}, \boldsymbol{v}_h). \qquad (19b)
\end{aligned}$$

Finally, let us mention that the motion of the computational mesh in the numerical examples of the forthcoming sections has been driven through the solution of an elastic problem [5]. Though efficient remeshing strategies are currently available (see e.g. [32]), they can be avoided if the deformations are not very large, which saves a considerable amount of computational cost.

5 Numerical Examples

5.1 Generation of a Sibilant /s/

As an example to show the performance of the proposed splitting strategy in the case of stationary domains (see Sect. 3.2), we will briefly summarize the results reported in [33] concerning the generation of sibilant fricative /s/. This sound is produced when the turbulent jet flow leaving the glottis becomes accelerated in the palatal constriction, passes through the incisors gap and finally impinges in the cavity between the lower incisors and the lower lips. In Fig. 2a, we can observe the portion of the vocal tract needed for the numerical production of /s/. A snapshot of the flow accelerating through the palatal constriction and impinging on the lower lips, which results in a highly developed turbulent flow, is shown in Fig. 2b. Figure 2c depicts the emission of acoustic wavefronts in a semi-hemisphere, which propagate outwards to infinity. Finally, in Fig. 2d we present the acoustic pressure for the total, incident

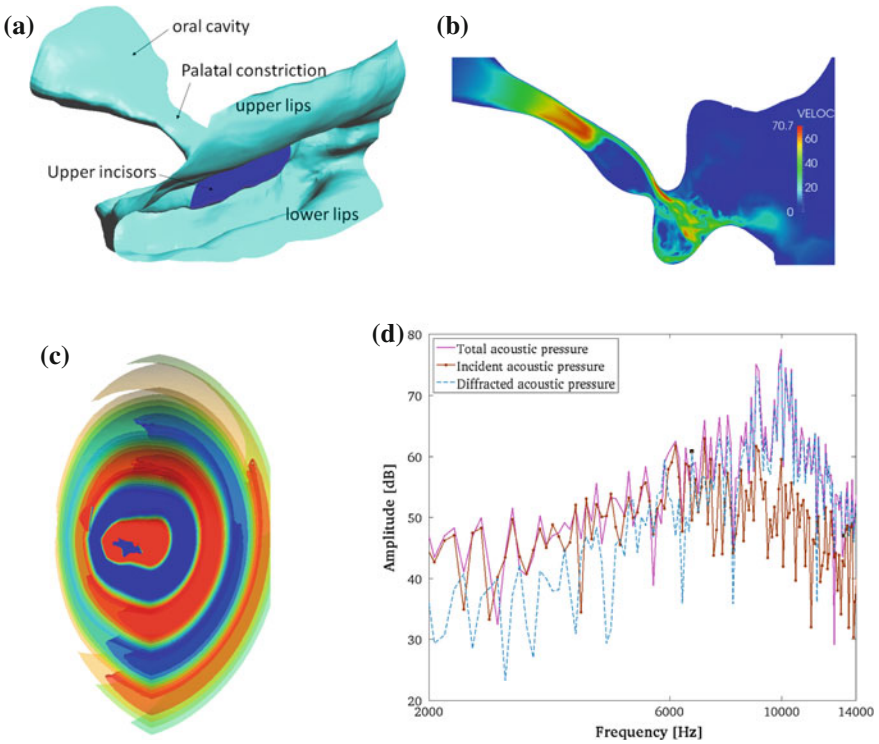

Fig. 2 Generation of sibilant /s/: **a** vocal tract geometry, **b** snapshot of the velocity profile, **c** acoustic front-waves, **d** spectra of the incident, diffracted and total acoustic pressure for a point at the far field

and diffracted acoustic pressure for a point located at the far field. The total pressure exhibits the typical wideband spectral content of an /s/ that usually peaks between 8–10 kHz, as observed on human speakers (see e.g. [16, 35]). The incident field directly originated by the flow motion dominates the spectrum up to 2 kHz; both the incident and diffracted components have similar contributions from 2 to 8 kHz, and the diffracted component dominates the spectrum for frequencies higher than 8 kHz.

The above three-dimensional simulations are computationally costly. To perform them, we have used a computational mesh of 45 million linear tetrahedral elements with equal interpolation for all variables. A total of three problems have been solved in the same finite element computational run (the incompressible Navier–Stokes equations plus the wave equations for the incident and diffracted acoustic pressure). A domain decomposition with an MPI distributed memory scheme has been carried out so as to run the problem at the MareNostrum computer cluster, of the Barcelona Supercomputing Centre (BSC). A period of 10.8 ms with a time step of $\Delta t = 5 \times 10^{-6}$ s has been simulated. The reader is referred to [33] for full details on the numerical simulations and the above-outlined results.

5.2 *Aeroacoustics of an Opening Teeth-Shaped Obstacle*

To demonstrate the extended splitting approach for domains with moving boundaries (see Sect. 3.3), and to test as well the numerical proposal in Sect. 4, we have considered a two-dimensional example. This consists of a duct with a teeth-shaped obstacle near to its exit, which evolves from a minimum opening of 3 mm to a maximum one of 18 mm (see Fig. 3). A velocity of $U_0 = 2.4$ m/s is imposed at the duct entrance and no-slip conditions are considered for the flow at the duct walls. The latter are also

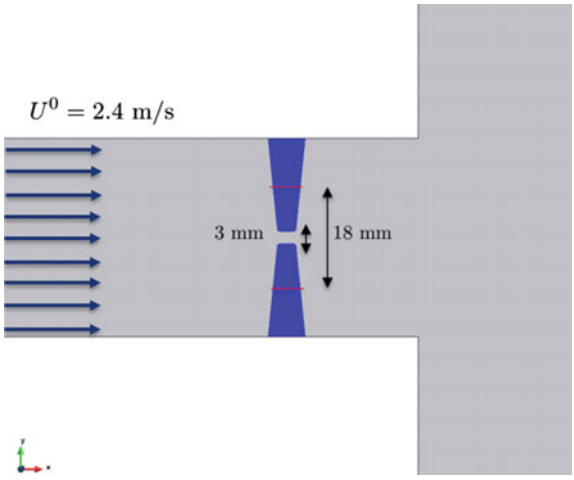

Fig. 3 Scheme of the computational domain close to the duct exit. The obstacle evolves from minimum to maximum opening

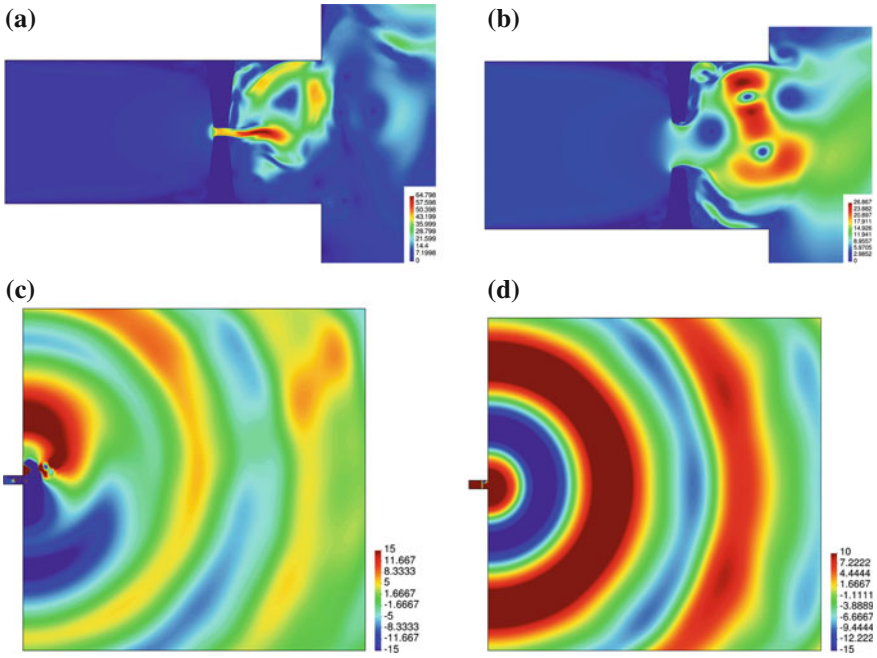

Fig. 4 Opening teeth-shaped obstacle: **a** velocity snapshot at minimum opening, **b** velocity profile at maximum opening, **c** incident acoustic pressure at minimum opening, **d** diffracted acoustic pressure at minimum opening

considered as being acoustically rigid, and a Sommerfeld non-radiating condition is imposed at the outer boundaries of the computational domain.

The results of the simulations are presented in Fig. 4. When the opening is minimum, an oscillating jet is developed after the obstacle, which results in the generation of intense flow noise after the obstacle. A snapshot of the velocity field at minimum opening is shown in Fig. 4a. As the teeth open, the jet stops oscillating and transitions to a fully developed turbulent flow, which radiates in a much weaker fashion (see Fig. 4b for a velocity snapshot at maximum opening). In Fig. 4c, we have plotted the incident pressure field for the minimum opening situation, when radiation is more intense, whereas a snapshot of the diffracted one is given in Fig. 4d. The diffracted component clearly dominates at the far field, as expected.

6 Conclusions

In this book chapter, we have first revisited a strategy for CAA at low Mach numbers, which allows one to compute the separate contributions of the incident flow noise, and of the noise diffracted by a stationary rigid body, on the acoustic pressure at

a point far away from the aeroacoustic sources. The strategy avoids some of the difficulties of Curle's analogy when resorting to incompressible computational fluid dynamics to compute the acoustic source terms, and only requires a single FEM code, as opposed to hybrid approaches to CAA. As an application, we have shown how the method could be used to produce a fricative sound like /s/, providing useful information of its underlying generation mechanisms.

Yet, the core of this work has consisted in extending the above approach to deal with aerodynamic sound generation in domains with moving boundaries. The standard irreducible wave equation has proved inadequate for such purposes, and the splitting strategy into incident and diffracted acoustic components has consequently been applied to the wave equation in mixed form. Hence, not only the pressure but also the acoustic particle velocity has become split into components. However, the Galerkin FEM for mixed problems is known to fail if an equal interpolation is used for both the acoustic pressure and velocity fields, so a stabilization approach has been presented to remedy this problem. Finally, an example consisting of a flow impinging on a teeth-shaped obstacle placed close to the exit of a duct, and transitioning from a minimum gap opening to a bigger one, has illustrated the potential of the formulation.

References

1. Badia, S., Codina, R., Espinoza, H.: Stability, convergence and accuracy of stabilized finite elements methods for the wave equation in mixed form. SIAM J. Numer. Anal. **52**, 1729–1752 (2014)
2. Bailly, C., Bogey, C.: Contributions of computational aeroacoustics to jet noise research and prediction. Int. J. Comput. Fluid Dyn. **18**(6), 481–491 (2004)
3. Bailly, C., Bogey, C., Gloerfelt, X.: Some useful hybrid approaches for predicting aerodynamic noise. Comptes Rendus Mécanique **333**(9), 666–675 (2005)
4. Bogey, C., Bailly, C., Juvé, D.: Numerical simulation of sound generated by vortex pairing in a mixing layer. AIAA J. **38**(12), 2210–2218 (2000)
5. Chiandussi, G., Bugeda, G., Oñate, E.: A simple method for automatic update of finite element meshes. Int. J. Numer. Method. Biomed. Eng. **16**(1), 1–19 (2000)
6. Codina, R.: Stabilized finite element approximation of transient incompressible flows using orthogonal subscales. Comput. Methods Appl. Mech. Eng. **191**, 4295–4321 (2002)
7. Codina, R.: Finite element approximation of the hyperbolic wave equation in mixed form. Comput. Methods Appl. Mech. Eng. **197**(13–16), 1305–1322 (2008)
8. Codina, R., González-Ondina, J., Díaz-Hernández, G., Principe, J.: Finite element approximation of the modified Boussinesq equations using a stabilized formulation. Int. J. Numer. Meth. Fluids **57**(9), 1249–1268 (2008)
9. Codina, R., Principe, J., Guasch, O., Badia, S.: Time dependent subscsales in the stabilized finite element approximation of incompressible flow problems. Comput. Methods Appl. Mech. Eng. **196**(21–24), 2413–2430 (2007)
10. Crighton, D.: Basic principles of aerodynamic noise generation. Prog. Aerospace Sci. **16**(1), 31–96 (1975)
11. Crighton, D., Dowling, A., Ffowcs Williams, J., Heckl, M., Leppington, F.: Modern Methods in Analytical Acoustics-Lecture Notes. Springer-Verlag (1992)
12. Curle, N.: The influence of solid boundaries upon aerodynamic sound. Proc. R. Soc. Lond. A **231**(1187), 505–514 (1955)

13. Doak, P.: Acoustic radiation from a turbulent fluid containing foreign bodies. Proc. R. Soc. Lond. A **254**(1276), 129–146 (1960)
14. Espinoza, H., Codina, R., Badia, S.: A Sommerfeld non-reflecting boundary condition for the wave equation in mixed form. Comput. Methods Appl. Mech. Eng. **276**, 122–148 (2014)
15. Ewert, R., Schröder, W.: Acoustic perturbation equations based on flow decomposition via source filtering. J. Comput. Phys. **188**(2), 365–398 (2003)
16. Fujiso, Y., Nozaki, K., Van Hirtum, A.: Towards sibilant physical speech screening using oral tract volume reconstruction: some preliminary observations. Appl. Acoust. **96**, 101–107 (2015)
17. Gloerfelt, X., Pérot, F., Bailly, C., Juvé, D.: Flow-induced cylinder noise formulated as a diffraction problem for low Mach numbers. J. Sound Vib. **287**(1), 129–151 (2005)
18. Guasch, O., Arnela, M., Codina, R., Espinoza, H.: A stabilized finite element method for the mixed wave equation in an ALE framework with application to diphthong production. Acta Acust. United Acust. **102**(1), 94–106 (2016)
19. Guasch, O., Codina, R.: An algebraic subgrid scale finite element method for the convected Helmholtz equation in two dimensions with applications in aeroacoustics. Comput. Methods Appl. Mech. Eng. **196**(45–48), 4672–4689 (2007)
20. Guasch, O., Codina, R.: Computational aeroacoustics of viscous low speed flows using subgrid scale finite element methods. J. Comput. Acoust. **17**(3), 309–330 (2009)
21. Guasch, O., Pont, A., Baiges, J., Codina, R.: Concurrent finite element simulation of quadrupolar and dipolar flow noise in low Mach number aeroacoustics. Comput. Fluids **133**, 129–139 (2016)
22. Guasch, O., Sánchez-Martín, P., Pont, A., Baiges, J., Codina, R.: Residual-based stabilization of the finite element approximation to the acoustic perturbation equations for low Mach number aeroacoustics. Int. J. Numer. Meth. Fluids **82**(12), 839–857 (2016)
23. Hueppe, A., Kaltenbacher, M.: Spectral finite elements for computational aeroacoustics using acoustic perturbation equations. J. Comput. Acoust. **20** (2), 1240005 (2012)
24. Huerta, A., Liu, W.: Viscous flow with large free surface motion. Comput. Methods Appl. Mech. Eng. **69**, 277–324 (1988)
25. Hughes, T.: Multiscale phenomena: Green's function, the dirichlet-to-neumann formulation, subgrid scale models, bubbles and the origins of stabilized formulations. Comput. Methods Appl. Mech. Eng. **127**, 387–401 (1995)
26. Hughes, T., Feijo, G., Mazzei, L., Quincy, J.: The variational multiscale method, a paradigm for computational mechanics. Comput. Methods Appl. Mech. Eng. **166**, 3–24 (1998)
27. Hughes, T., Liu, W., Zimmermann, T.: Lagrangian-eulerian finite-element formulation for compressible viscous flows. Comput. Methods Appl. Mech. Eng. **29**, 329–349 (1981)
28. Kaltenbacher, M., Escobar, M., Becker, S., Ali, I.: Numerical simulation of flow-induced noise using LES/SAS and lighthill's acoustic analogy. Int. J. Numer. Meth. Fluids **63**(9), 1103–1122 (2010)
29. Lighthill, M.J.: On sound generated aerodynamically I. General theory. Proc. R. Soc. Lond. A **211** (1107), 564–587 (1952)
30. Morse, P.M., Ingard, K.U.: Theoretical Acoustics. McGraw-Hill, New York (1968)
31. Oberai, A.A., Roknaldin, F.R., Hughes, T.J.: Computation of trailing-edge noise due to turbulent flow over an airfoil. AIAA J. **40**(11), 2206–2216 (2002)
32. Pont, A., Codina, R., Baiges, J.: Interpolation with restrictions between finite element meshes for flow problems in an ALE setting. Int. J. Numer. Meth. Eng. **110**(13), 1203–1226 (2017)
33. Pont, A., Guasch, O., Baiges, J., Codina, R., Van Hirtum, A.: Computational aeroacoustics to identify sound sources in the generation of sibilant /s/. Submitted (2017)
34. Roger, M.: Aeroacoustics: some theoretical background–The acoustic analogy, Anthoine, J., Colonius, T. (Eds.), vol. LS 2006-05. Von Karman Institute, Rhode-St-Genese (2006)
35. Van Hirtum, A., Fujiso, Y., Nozaki, K.: The role of initial flow conditions for sibilant fricative production. J. Acoust. Soc. Am. **136**(6), 2922–2925 (2014)
36. Williams, J.F., Hawkings, D.L.: Sound generation by turbulence and surfaces in arbitrary motion. Phil. Trans. Roy. Soc. A **264**(1151), 321–342 (1969)